Sulfur-Bridged Terthiophene Dimers: How Sulfur Oxidation State Controls Interchromophore Electronic Coupling

Chad D. Cruz,[§,||] Peter R. Christensen,[‡,||] Eric L. Chronister,[§] David Casanova,*[#,⊥] Michael O. Wolf,*[‡] and Christopher J. Bardeen*[§]

[§]Department of Chemistry, University of California Riverside, 501 Big Springs Road, Riverside, California 92521, United States
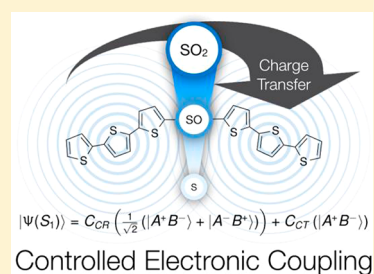
[‡]Department of Chemistry, University of British Columbia, 2036 Main Mall, Vancouver, British Columbia V6T 1Z1 Canada

[#]Kimika Facultatea, Euskal Herriko Unibertsitatea (UPV/EHU), Donostia International Physics Center, P.K: 1072, Donostia 20080, Spain

[⊥]IKERBASQUE, Basque Foundation for Science, Bilbao, Euskadi 48013, Spain

S *Supporting Information*

ABSTRACT: Symmetric dimers have the potential to optimize energy transfer and charge separation in optoelectronic devices. In this paper, a combination of optical spectroscopy (steady-state and time-resolved) and electronic structure theory is used to analyze the photophysics of sulfur-bridged terthiophene dimers. This class of dimers has the unique feature that the interchromophore (intradimer) electronic coupling can be modified by varying the oxidation state of the bridging sulfur from sulfide (S), to sulfoxide (SO), to sulfone (SO_2). Photoexcitation leads to the formation of a delocalized charge resonance state (S_1) that relaxes quickly (<10 ps) to a charge-transfer state (S_1*). The amount of charge-transfer character in S_1* can be enhanced by increasing the oxidation state of the bridging sulfur group as well as the solvent polarity. The S_1* state has a decreased intersystem crossing rate when compared to monomeric terthiophene, leading to an enhanced photoluminescence quantum yield. Computational results indicate that electrostatic screening by the bridging sulfur electrons is the key parameter that controls the amount of charge-transfer character. Control of the sulfur bridge oxidation state provides the ability to tune interchromophore interactions in covalent assemblies without altering the molecular geometry or solvent polarity. This capability provides a new strategy for the design of functional supermolecules with applications in organic electronics.

$$|\Psi(S_1)\rangle = C_{CR}\left(\frac{1}{\sqrt{2}}\left(|A^+B^-\rangle + |A^-B^+\rangle\right)\right) + C_{CT}\left(|A^+B^-\rangle\right)$$

Controlled Electronic Coupling

1. INTRODUCTION

In nature, light harvesting organisms make extensive use of energy and electron transfer between adjacent molecules. A great deal of work has been focused on synthesizing electron donor/acceptor pairs to mimic these efficient natural systems. The most common approach is to unite an electron-rich donor with an electron-deficient acceptor using a π-conjugated linkage or "bridge." Separation of the donor and acceptor by such a bridge can enable charge transfer (CT) over large distances, limiting charge recombination.[1] While remarkable photovoltaic performance has been achieved using this approach,[2] these asymmetric systems only partially mimic the naturally occurring photosynthetic reaction centers, where symmetric chromophore pairs have a central role in controlling excited-state dynamics.[3,4]

The rational design of symmetrically bridged chromophore dimers, also called bichromophores, has attracted considerable theoretical[5,6] and practical[7,8] interest. For example, 9,9′-bianthryl, where two anthracene units are covalently bonded and adopt a nearly orthogonal orientation, has served as a model system for the study of excited-state electron transfer.[9] Recently, Thompson et al. have synthesized a series of symmetric dipyrrin molecules that exhibit symmetry breaking CT using visible light.[10−12] These symmetric CT systems are of practical interest because the CT and neutral states are close in energy, which lowers the amount of energy lost in the charge separation event and has the potential to raise the open-circuit voltage of photovoltaic devices.

Bichromophoric systems have also found applications in organic light emitting diodes (OLEDs).[13,14] Recently, Adachi et al. synthesized several types of organic molecules that harness both singlet and triplet excitons through a process known as thermally activated delayed fluorescence (TADF).[15,16] The singlet−triplet energy gap is most efficiently reduced when the HOMO and LUMO are spatially separated, which can be facilitated by intramolecular CT.[17] High-efficiency blue OLEDs were fabricated using SO_2-bridged symmetric bichromophores.[18,19] While it was demonstrated that these SO_2-bridged chromophores exhibit reduced singlet−triplet gaps facilitated by CT, the role of the symmetric nature of these emitters was not investigated.

It is anticipated that applications of dimeric molecules in photovoltaic and light emitting devices will require precise control of intradimer electronic interactions. One control strategy is to change the polarity of the environment and shift

the relative energy levels of neutral and CT states; however, in solid-state devices, this is impractical. An alternate strategy is to control the electronic coupling between light absorbing units. Ideally, such a control element would be built into the dimer molecule itself, without inducing large conformational changes. Decreasing the distance and angle between chromophores can enhance electron transfer, but if molecules are too close together, aggregation-induced excited-state quenching often results.[20] The goal is then to control the interchromophore coupling while maintaining ideal dimer geometry.

Recently, we demonstrated that bridging two conjugated chromophores symmetrically about a sulfur atom results in systematic enhancement of the photoluminescence (PL) by oxidizing the bridging sulfur.[21] Increasing the oxidation state of the sulfur bridge also resulted in pronounced red-shifts of the PL spectra in polar solvents, an indication of increasing CT character. The observation that simply linking two terthiophenes together could lead to new CT excited states and increase the PL yield by an order of magnitude raised several questions regarding the origin of the changes in spectroscopic behavior. The first question concerns the role of the sulfur linker: Does it actively participate in the electronic states, and why does its oxidation state have such a large effect? Related to this question, one may ask whether the second chromophore plays an important role. If the CT state involves only one of the terthiophene groups and the bridging sulfur, then perhaps the second terthiophene is not even necessary. The question of electronic structure is intimately related to the excited-state dynamics: How is the CT state formed and why is its relaxation different from that of a single chromophore? This class of sulfur-bridged terthiophene dimers, with potential applications in organic electronics, provides an ideal model system in which to study fundamental questions about the excited-state behavior in symmetric bichromophore systems.

In this paper, we use optical spectroscopy (steady-state and time-resolved) and electronic structure theory to develop a complete picture of the photophysics of the terthiophene derivatives shown in Chart 1. We find that the bridge itself does

Chart 1. Terthiophene Derivatives Studied in This Work
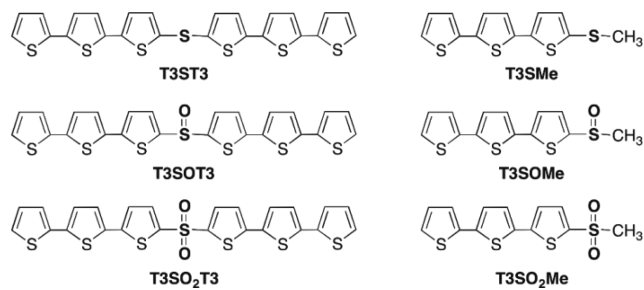
not significantly affect the excited-state structure, but the oxidation state of the sulfur bridge mediates the amount of electronic coupling between the two terthiophene chromophores. Using femtosecond transient absorption (TA) experiments, we show that the initially excited state is a delocalized excitonic state with an overall neutral character that relaxes within 10 ps to a second state, where the CT character depends on the bridge oxidation state. This CT state has different radiative and intersystem crossing (ISC) rates when compared to monomeric terthiophene. Based on computational results, we propose a mechanism in which electrostatic screening by

lone pairs on the sulfur linker controls the CT character of the excited-state wave function. Our results suggest that it is possible to use electron density on the bridge to mediate intramolecular interactions and tune the electronic coupling between identical chromophores without altering the dimer geometry or solvent polarity. The results of this paper not only reveal the origins of the novel properties of a specific class of terthiophene bichromophores but also provide new directions for the design of symmetric chromophore systems that may find applications in fields ranging from artificial photosynthesis to organic electronics.

2. EXPERIMENTAL SECTION

2.1. Synthesis and Sample Preparation. All of the sulfur-bridged terthiophene dimers (**T3SO$_n$T3**, where n = 0, 1, 2) used in this study were synthesized according to previously reported methods.[21] An appropriate model "monomer" was synthesized by replacing the second terthiophene molecule with a methyl group (**T3SO$_n$Me**) (see Supporting Information for synthetic details). The structures of the monomer and dimer compounds are shown in Chart 1.

2.2. Spectroscopy. *2.2.1. Steady-State UV−vis/Emission.* Electronic absorption spectroscopy was performed on a Varian Cary 5000 spectrophotometer. Corrected emission measurements were performed on a PTI QuantaMaster 50 fluorimeter at room temperature, unless otherwise specified.

2.2.2. Time-Resolved Spectroscopy. Time-resolved PL lifetime experiments were performed by frequency doubling the 750 nm output of a tunable Ti:sapphire Mai Tai laser to generate the excitation wavelength (375 nm) or using the 400 nm output of the 1 kHz laser system described below. Spectra were recorded with a Hamamatsu C4334 Streakscope which has a time resolution of 15 ps and wavelength resolution of 2.5 nm. The spectra were collected in a front face configuration utilizing magic angle polarization.

TA measurements were performed using a 1 kHz Coherent Libra laser system with an Ultrafast Systems Helios TA spectrometer. The pump beam (400 nm) was generated by frequency doubling the fundamental 800 nm output. A small portion of the fundamental beam was focused onto a 3 mm sapphire plate to generate the white-light continuum probe beam. The pump and probe beams were focused onto the same spot on a 1 mm path length, quartz flow cell. A 4 cm focal length lens was used to collect the scattered probe beam which was then coupled into an Ocean Optics S2000 spectrometer. Nonresonant contributions to the TA signal were removed by measuring each solvent response under the same experimental conditions and were subtracted from the signal using Ultrafast Systems Surface Xplorer software.[22] Pump fluences for each TA measurement were kept between 20 and 200 μJ/cm^2.

2.3. Computational Details. Electronic structure calculations of terthiophene (**T3**), **T3SO$_n$Me**, and **T3SO$_n$T3** molecules were performed using density functional theory (DFT)[23,24] with the long-range corrected version of B3LYP energy functional (CAM-B3LYP).[25] Electronic transitions were obtained with the time-dependent version of DFT (TDDFT)[26,27] and with the Tamm−Dancoff approximation.[28,29] The 6-31G(d) and 6-31+G(d) basis sets were employed for molecular geometry optimizations and the computation of excitation energies to low-lying states, respectively. The B3LYP energy functional has shown good performance in the computation of electronic excitations of sulfur-organic compounds.[30] Although it is often advisable to use tight d-functions to account for core polarization effects when dealing with second row elements such as sulfur, we found that our chosen atomic basis functions gave similar optimized geometries and transition energies (Table S7 and Figure S28). One of the main limitations of TDDFT is its difficulty with CT-type excitations. For this reason, we have used the long-range corrected version of the B3LYP energy functional CAM-B3LYP, which has shown to be capable of reliably computing CT transitions in organic molecules.[31−33]

The effect of the solvent was taken into consideration in all calculations with the polarizable continuum model (PCM).[34] Diabatic states have been constructed with the Edmiston−Ruedenberg localization scheme[35] as linear combinations from the four lowest excited singlet eigenstates. Coupling energies between locally excited (LE) and CT diabats correspond to off diagonal terms of the four by four diabatic Hamiltonian. All calculations were done using the Q-Chem program.[36] Natural bond orbital (NBO) analysis was performed at the CAM-B3LYP/6-31+G(d) level in dichloromethane with the NBO 5.0 package.[37]

3. RESULTS

3.1. Spectroscopy. *3.1.1. Steady-State Absorption Spectroscopy.* The experimental absorption spectra of **T3**, **T3SO$_2$Me**, and **T3SO$_2$T3** in dichloromethane are shown in Figure 1. When a methyl-terminated SO$_2$ linker is added to **T3**,
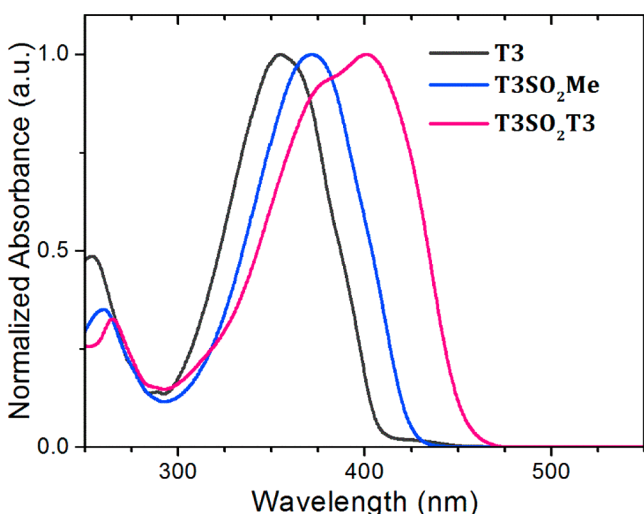
Figure 1. UV−vis spectra for unsubstituted terthiophene (**T3**), monomer (**T3SO$_2$Me**), and dimer (**T3SO$_2$T3**) all in dichloromethane.

the absorption peak shifts from 350 to 370 nm, but the overall peak shape remains the same, and there is no discernible broadening. The same is true for the S and SO linkers (Figure S5). When the methyl group is replaced by a second **T3** (**T3SO$_2$T3**), the absorption not only redshifts farther but also broadens considerably, with two distinguishable peaks at 400 and 375 nm. This change in the absorption line shape is the first clue that the **T3−T3** electronic interaction plays an important role. Similar changes in absorption lineshapes are observed for the **T3ST3** and **T3SOT3** dimers. Since the lowest-energy transition for all **T3SO$_n$T3** species (∼400 nm) is higher in energy than that of sexithiophene (∼435 nm),[38,39] the electronic interactions in these dimers are not as strong as in a fully conjugated system. Although the absorption spectra are sensitive to the presence of the second **T3**, they are not very sensitive to solvent polarity.[21]

The splitting of the dimer absorption spectra likely originates from through-space Coulombic interactions between the two **T3** chromophores. The two bands observed in the absorbance spectra of **T3SO$_n$T3** are attributed to interacting transition dipoles of the two monomers resulting in exciton splitting.[40,41] The low-energy bands in the absorption spectra of the **T3SO$_n$T3** dimers can be fit using a pair of Gaussians, allowing us to estimate values for the excitonic splitting energy Δε (Figure S7). The splitting Δε increases with sulfur oxidation

state (Δε = 1870 cm^{-1} for **T3ST3**, Δε = 2050 cm^{-1} for **T3SOT3**, and Δε = 2150 cm^{-1} for **T3SO$_2$T3**). This interaction is slightly smaller than the H-type aggregate coupling typically seen in oligothiophene crystals, in which the chromophores have an approximately parallel orientation.[42] We can estimate the exciton splitting energy Δε in each of the absorption spectra by using eq 1 to describe the interaction of two point dipoles A and B:

$$\Delta\varepsilon = \frac{2\,|\mu|^2}{|\vec{r}_{AB}|^3}(\cos\alpha + 3\cos^2\theta) \tag{1}$$

where μ is the transition dipole moment, $\vec{r}_{AB}$ is the center-to-center vector between dipoles, α is the angle between the dipoles, and θ is the angle between the transition dipole moment and $\vec{r}_{AB}$ (Table S2 and Figure S6). Using eq 1, with values of $\vec{r}_{AB}$, α, and θ (from computational results and X-ray crystallographic data)[21,43] and μ for unsubstituted terthiophene,[44] we calculate Δε = 2000 cm^{-1} for **T3ST3**, Δε = 2100 cm^{-1} for **T3SOT3**, and Δε = 1900 cm^{-1} for **T3SO$_2$T3**. All the values are close to 2000 cm^{-1}, consistent with the experimental results. This is somewhat surprising, considering that the point-dipole approximation of eq 1 tends to overestimate Δε for chromophores in close proximity.[45−48] The calculations predict no systematic increase in Δε from **T3ST3** to **T3SO$_2$T3** because the molecular geometries are quite similar. However eq 1 only considers through-space dipole−dipole interactions, and it is known that electron-transfer terms can also contribute to excitonic splittings.[47,49−52] Comparing the calculated exciton splitting energy with those determined experimentally, it appears that such electron-transfer contributions to Δε may play a larger role as the sulfur oxidation state is increased.

3.1.2. Steady-State and Time-Resolved Photoluminescence. The steady-state PL spectra of **T3SO$_2$Me** and **T3SO$_2$T3** are compared in nonpolar cyclohexane, moderately polar dichloromethane, and highly polar acetonitrile (Figure 2). Increasing the solvent polarity for the monomer (**T3SO$_2$Me**) solutions results in only a small red-shift, with no change observed between moderately polar dichloromethane and polar acetonitrile (Figure 2A). Similar behavior is observed for the S and SO linkers (Figure S8). When the dimer (**T3SO$_2$T3**) is examined, however, an ∼100 nm red shift in the PL maximum is observed when the solvent polarity is increased from nonpolar cyclohexane to highly polar acetonitrile (Figure 2B). The different solvatochromic behaviors are accompanied by different fluorescence lineshapes. In acetonitrile, the fluorescence spectra of the **T3SO$_n$Me** monomer series hardly change from those in dichloromethane. In the same solvent, the dimers (**T3SO$_n$T3**) display relatively broad and unstructured profiles. These results reinforce our earlier conclusions that while the absorption spectra of **T3SO$_n$T3** are relatively insensitive to solvent, the fluorescence spectra of the dimers exhibit strong solvatochromism.[21] The new results with the **T3SO$_n$Me** monomers demonstrate that the CT character of the emitting state arises from the presence of the second **T3** chromophore and not from the linker itself. Finally, the degree of dimer solvatochromism depends on the linker oxidation state, with the SO$_2$ linker showing the largest shift and the S linker showing much smaller shifts.
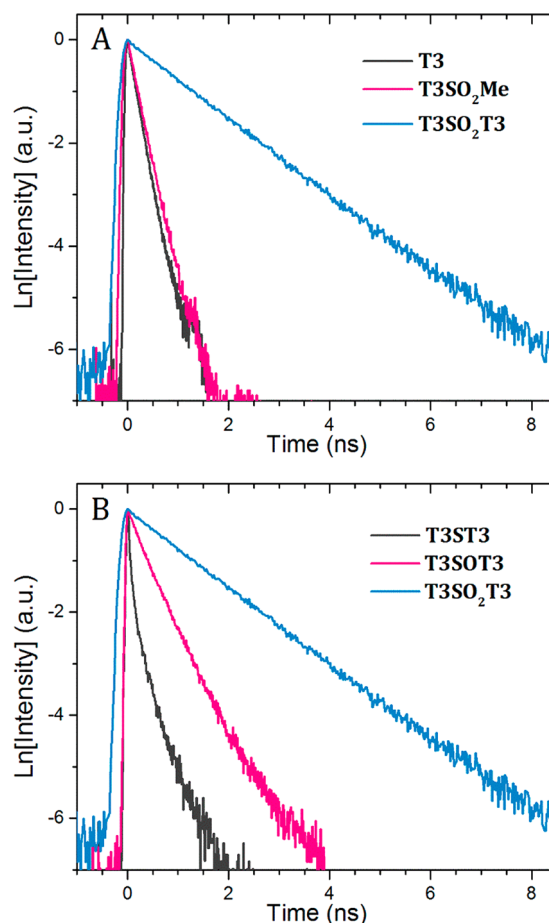
Unsubstituted **T3** has a relatively short PL lifetime (τ_{PL} = 190 ps), due to rapid ISC to its triplet state.[53,54] When the SO$_n$Me group is added, the PL lifetimes change very little. The
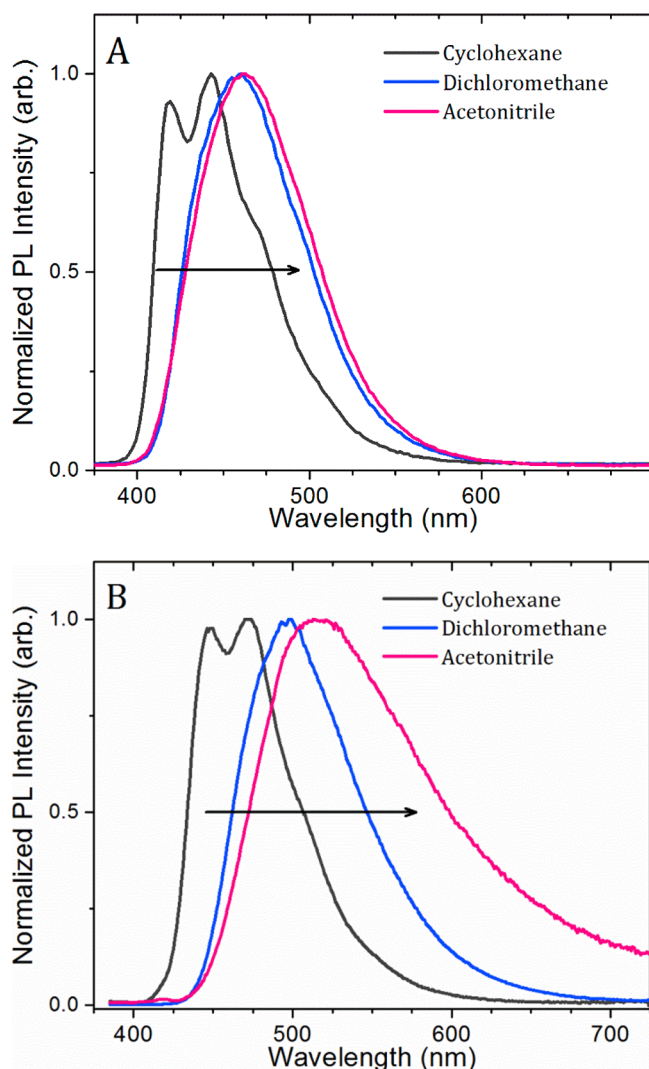
Figure 2. PL spectra for **T3SO₂Me** (A) and **T3SO₂T3** (B) in increasingly polar solvents from left to right (→) cyclohexane, dichloromethane, and acetonitrile.

Figure 3. Fluorescence decays illustrating the effect of adding a second chromophore to the bridge (A) and comparing the oxidation states of the bridging sulfur for the bichromophoric compounds (B) all in dilute solutions of dichloromethane.

monomers in dichloromethane have a τ_{PL} which varies only slightly depending upon the oxidation state of the sulfur, with a slight increase observed with increasing oxidation (171 ps for **T3SMe**, 195 ps for **T3SOMe**, and 219 ps for **T3SO₂Me**). The lifetimes are not appreciably different from that of unsubstituted **T3** and do not exhibit a strong solvent dependence (Figures S9 and S10).

When the terminal methyl substituent is changed to **T3**, however, there is a significant increase in the fluorescence lifetime, as shown in Figure 3a. The different bridge oxidation states also give rise to different lifetimes in the dimers, as shown in Figure 3b. In all solvents, the lifetimes of the unoxidized sulfur-bridged dimer **T3ST3** are consistently shorter than those of the sulfoxide **T3SOT3**, which in turn are shorter than those of the sulfone **T3SO₂T3**. Of the compounds studied, only **T3ST3** deviated from monoexponential decay behavior, requiring a minor (~15%) second component when fit to a biexponential function. A stretched exponential function could also be used, but since there is some evidence that two different conformers may be present (see Theory section), a biexponential is more justified physically. Despite this

complication, the average fluorescence lifetime of **T3ST3** fits well with the trend observed in Figure 3.

The radiative lifetime τ_{rad} of **T3SO₂T3** (Table 1) increases with solvent polarity, consistent with a loss of oscillator strength in more polar solvents. This decrease in oscillator strength is concordant with an increasing degree of charge separation and is another hallmark of a CT state.[55,56] The effect

Table 1. PL Quantum Yields (Φ_{PL}), PL Lifetimes (τ_{PL}), and Radiative Rates (τ_{rad}) for T3SO$_n$T3 in Various Solvents

|		molecule		
solvent	parameter	T3ST3	T3SOT3	T3SO₂T3
acetonitrile	Φ_{PL}	0.007	0.026	0.137
	τ_{PL} (ps)	120.8[a]	270.0	646.5
	τ_{rad} (ps)	1948	10385	4719
dichloromethane	Φ_{PL}	0.012	0.173	0.565
	τ_{PL} (ps)	87.1[b]	405.3	1382.1
	τ_{rad} (ps)	7256	2343	2446
cyclohexane	Φ_{PL}	—	—	0.138
	τ_{PL} (ps)	—	—	264.7
	τ_{rad} (ps)	—	—	1918

[a]Weighted average of two components (58.7 ps (86%) and 475.3 ps (14%)). [b]Weighted average of two components (49.2 ps (85%) and 297.8 (15%)).

of the oxidation state of the bridging sulfur group on the emission lifetime is similar for both the monomers and dimers, in that increasing the oxidation state from S to SO_2 results in an increase in the observed τ_{PL}. However, the trend is much more pronounced in the bridged dimers. The PL lifetimes (τ_{PL}) and relevant spectroscopic parameters of the terthiophene compounds are summarized in Table 1. In general, a higher oxidation state for the bridge leads to a more pronounced solvatochromic character of the emitting state as well as longer lifetimes and higher quantum yields.

3.1.3. Femtosecond Transient Absorption. The results presented in the preceding sections indicate that the excited-state character of the dimers changes between the absorption and emission events. The absorbing state has an overall neutral character, as inferred from its lack of solvatochromism. The emitting state, on the other hand, has pronounced CT character that is strongly influenced by both solvent polarity and the oxidation state of the bridge. In order to understand how these two excited states are connected, TA measurements were performed.

The femtosecond TA of unsubstituted **T3** in solution has been measured previously.[57] In this molecule, an initial singlet $S_1 \rightarrow S_n$ excited-state absorption in the visible decays to a signature $T_1 \rightarrow T_n$ triplet absorption on the same time scale as the PL decay. The photophysical behavior is consistent with that of a simple three-state system: absorption from S_0 to S_1, followed by ISC from S_1 to T_1 on the 190 ps time scale. The T_1 state then survives for nanoseconds before decaying back to S_0. The TA spectra of the **T3SO$_n$Me** monomers show similar behavior. At early times ($t < 100$ ps), the **T3SO$_2$Me** monomer shows a negative feature at 490 nm (Figure 4a), corresponding to stimulated emission, as well as a positive feature at ~595 nm assigned to the singlet induced absorption ($S_1 \rightarrow S_n$). At longer times ($t > 100$ ps), the triplet induced absorption ($T_1 \rightarrow T_n$) grows in at ~500 nm, while the $S_1 \rightarrow S_n$ feature and the stimulated emission both decay. We assign the positive feature at 500 nm to the triplet since in **T3** the $T_1 \rightarrow T_n$ absorption is located at ~470 nm.[57,58] The redshift of the $T_1 \rightarrow T_n$ feature is expected because the T_n states tend to be less localized than T_1 and undergo a greater bathochromic shift upon substitution with electron-donating and -withdrawing groups.[59] The spectra in Figure 4a show an approximate isosbestic point, located at 545 nm, that suggests that the dominant relaxation process occurs between two well-defined electronic states. Using a principal component analysis, combined with a global fitting algorithm, we find that the data in Figure 4a can be described using three components linked by two relaxation times $\tau_1 = 30$ ps and $\tau_2 = 219$ ps. The latter time is just the measured fluorescence decay time and reflects the ISC time in this molecule. The 30 ps time describes a small shift in the $S_1 \rightarrow S_n$ absorption peak and probably reflects conformational relaxation or solvent reorganization. The amplitude of the pre-exponential factor that corresponds to this time is <20% of the initial component. In Figure 4b, we show the global amplitudes of the three components that contribute to the signal along with their decay times. The agreement with the data is very good at different probe wavelengths (Figure S13).

In the **T3SO$_n$T3** dimers the behavior is more complicated. All three compounds in dichloromethane show a much broader $S_1 \rightarrow S_n$ absorption that extends from the visible through the near-infrared, with a peak at ~600 nm and a second feature near 750 nm (Figures 5 and S12). As in the methyl-terminated compounds, the $S_1 \rightarrow S_0$ stimulated emission around 490 nm is
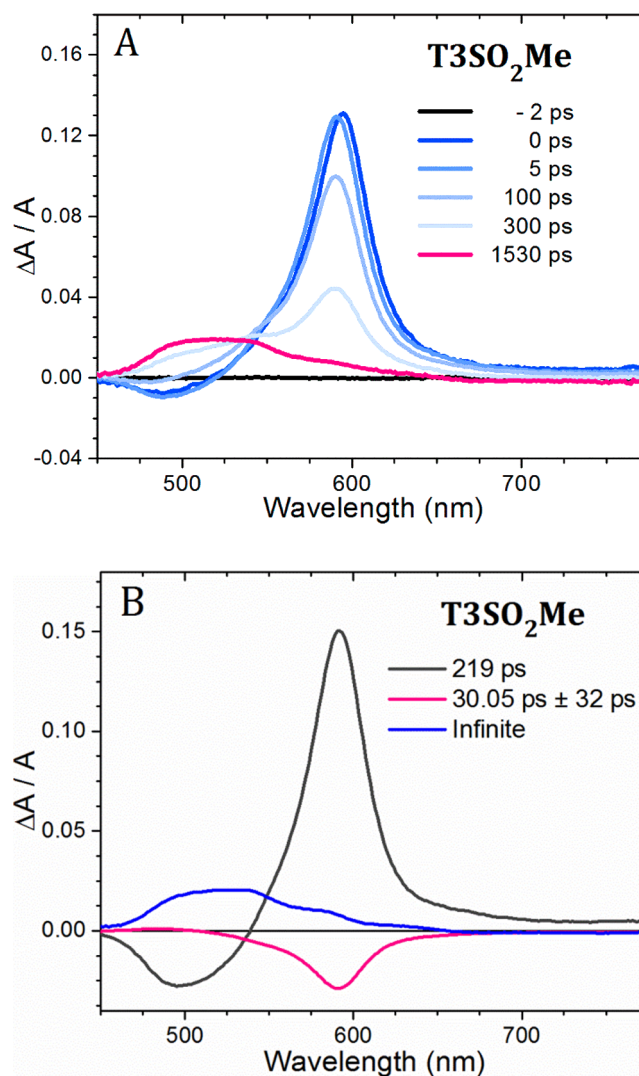
Figure 4. TA spectra (A) of **T3SO$_2$Me** in dichloromethane with the corresponding pre-exponential amplitudes obtained from the global fitting analysis (B).

eventually replaced by an induced absorption that is assigned to the triplet $T_1 \rightarrow T_n$ transition. For all three compounds, however, there is no clear isosbestic point because the induced absorption at 600 nm undergoes a rapid blueshift which is much more pronounced than in the monomer. For all three dimers, global analysis required a minimum of three components with two time constants. There is a fast (5−10 ps) component, followed by a slower component where the relaxation time mirrors the fluorescence decay time. The third component is strongly peaked around 500 nm, suggesting that it is associated with the triplet state T_1. In all three dimers, the fast component is comparable in magnitude to the other components, unlike in the monomer, where it leads only to a small spectral shift. The TA kinetic parameters for the dimers **T3SO$_n$T3** and the sulfone-bridged monomer **T3SO$_2$Me** in dichloromethane are summarized in Table 2. The important conclusion is that excited-state relaxation in the dimers appears to occur in two steps: fast relaxation from the absorbing state S_1 to an intermediate state S_1^*, followed by slower relaxation from S_1^* to the T_1 and S_0 states. The fluorescence behavior of the dimers is dominated by the relatively long-lived S_1^* state.
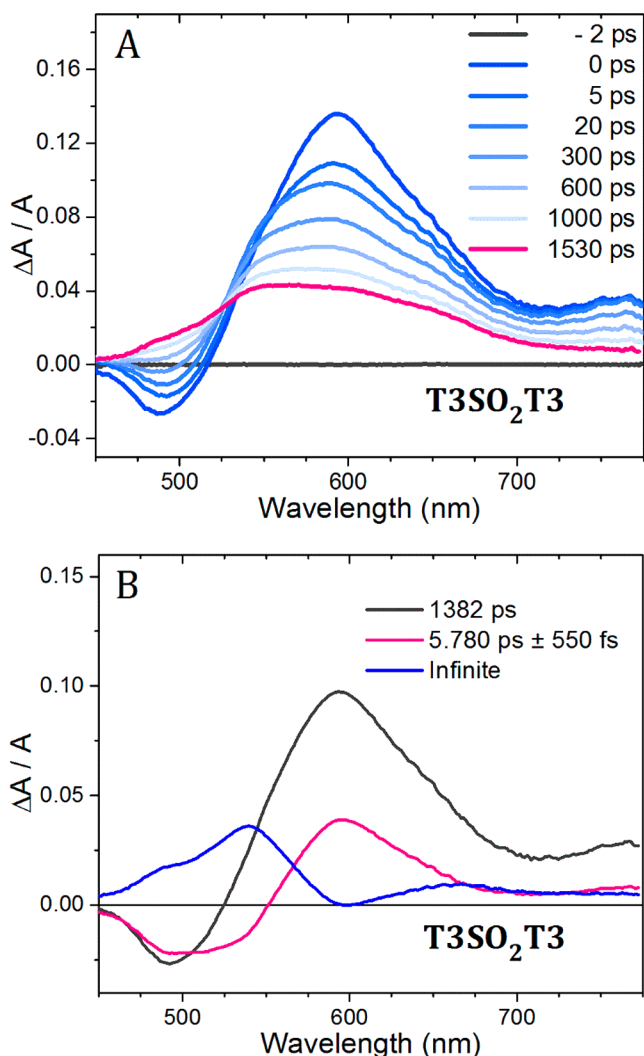
Figure 5. TA spectra of **T3SO₂T3** (A) in dichloromethane with the corresponding pre-exponential amplitudes obtained from the global analysis fit (B).

Table 2. TA Lifetimes Determined from the Global Fitting Analysis of the Principal Components for T3SO$_n$T3 and T3SO$_2$Me in Dilute Dichloromethane Solutions

	molecule			
	T3ST3	**T3SOT3**	**T3SO$_2$T3**	**T3SO$_2$Me**
τ_1 (ps)	5.42	8.65	5.78	30.05
τ_2 (ps)	49	405	1382	219

The solvent polarity was varied in order to probe the CT character of the S$_1$* intermediate state. There is little dependence upon solvent polarity observed in the TA spectra of the monomers (Figure S11). The spectral evolution of **T3SO$_2$T3** in nonpolar cyclohexane (Figure 6) is strongly reminiscent of that seen in **T3SO$_2$Me**, albeit with a broader S$_1$ → S$_n$ absorption feature that extends into the near-infrared region. There is a recognizable isosbestic point located at 530 nm as the T$_1$ → T$_n$ absorption grows in. A global fitting analysis yields only two components linked by a relaxation time of 265 ps, the experimentally measured fluorescence lifetime. The single wavelength traces in Figure 6b show only a decay and concomitant rise in the T$_1$ → T$_n$ absorption. Thus, in nonpolar
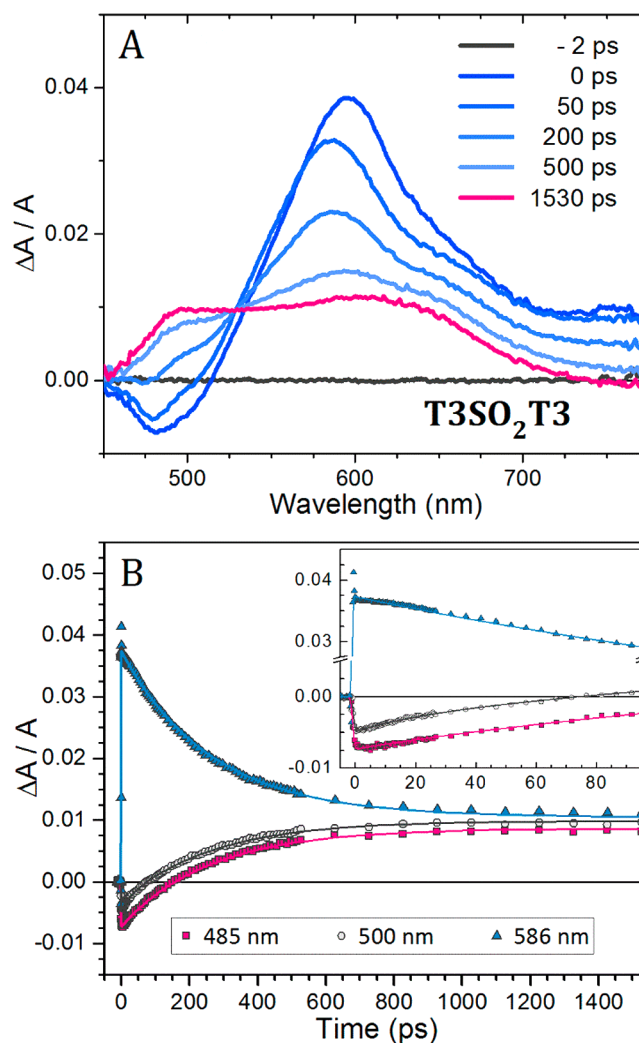

Figure 6. TA spectra of **T3SO$_2$T3** in cyclohexane (A) and the corresponding single wavelength kinetic traces and fits (B).

cyclohexane, **T3SO$_2$T3** behaves like monomeric **T3** and the methyl-terminated bridge compounds with a one-step population transfer between S$_1$ and the triplet manifold.

The dynamics are qualitatively different for **T3SO$_2$T3** in acetonitrile (Figure 7). In this solvent, a clear isosbestic point is also observed, now shifted to 570 nm. A global analysis of the two principal spectral components yields three fit parameters. The amplitude of the pre-exponential coefficient that corresponds to the isosbestic point at 570 nm is peaked at 525 nm and forms within 2.8 ± 1.1 ps. This feature then decays with the measured fluorescence lifetime of 646 ps. The rapid growth of the intermediate state can also be seen in the single wavelength traces in Figure 7b, where a clear increase in the signal is resolved at 530 nm, which then decays on a much slower time scale, close to the fluorescence decay time.

Comparing the cyclohexane and acetonitrile data, it seems that the energetic separation of S$_1$* from S$_1$ depends on solvent polarity and that, in the most polar solvent (acetonitrile), relaxation to the S$_1$* state leads to the appearance of a distinct electronic absorption feature. S$_1$* must correspond to a state with a high degree of charge separation that is stabilized by the surrounding medium. This S$_1$* state is most pronounced for **T3SO$_2$T3**. Similar relaxation dynamics are observed for **T3ST3** and **T3SOT3** in acetonitrile: the intermediate S$_1$* states are
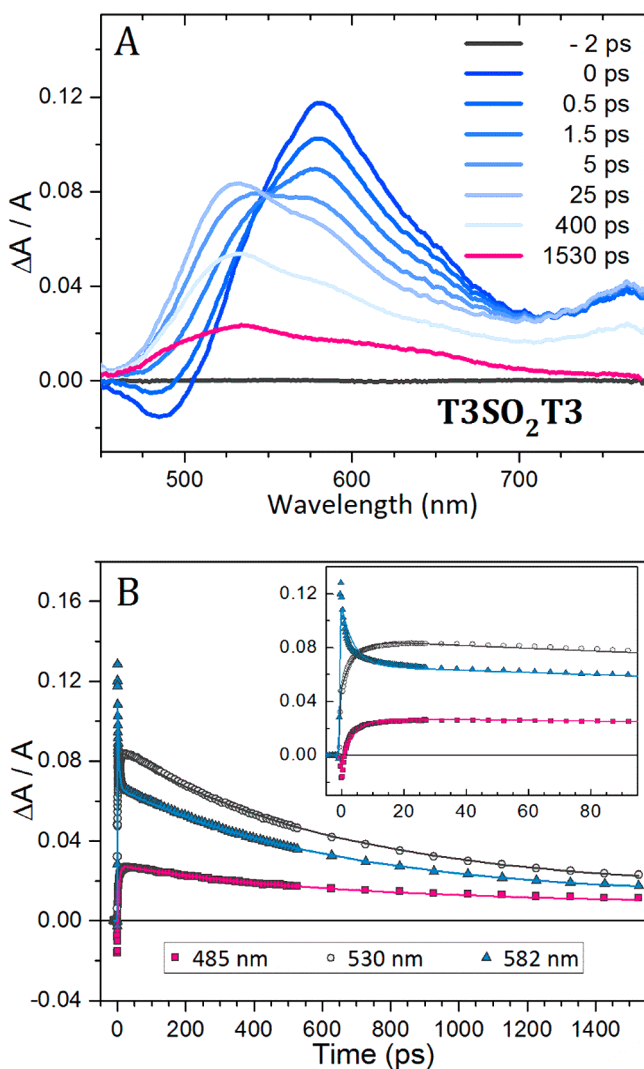
Figure 7. TA spectra of **T3SO₂T3** in acetonitrile (A) and the corresponding single wavelength kinetic traces and fits (B). Inset shows the early time (100 ps) evolution of traces with fits.

formed on comparable time scales (3.4 and 4.7 ps, respectively) but are not as pronounced spectrally (Figures S14–S20).

3.2. Theory. In order to gain insight into the nature of the dimer excited states, we used TDDFT calculations. One concern is that the molecules used in this study are relatively large and incorporate flexible linkers, which could lead to conformational disorder and distributed kinetic behavior. To address this concern, we computed the ground-state potential energy surfaces for bending and torsion of the dimers (Figure S29). In all cases the barriers are substantially higher than kT, the thermal energy. Note that even though the barriers to rotation are high, the energy difference between rotational conformers (*cis* and *trans*) can be small, which is why we consider both when calculating excitonic energy splittings. The fact that almost all the fluorescence decays and TA data in the preceding section could be fit with single exponentials provides experimental evidence that the spectroscopic behavior of these conformers must be quite similar. The only exception is the **T3ST3** dimer, which had a minor (~15%) long-lived component in its fluorescence decays, suggesting that *cis* and *trans* isomers may have different relaxation dynamics in this molecule. Overall, both experiment and theory suggest that

conformational disorder does not play a decisive role in the observed dynamics.

We are particularly interested in the nature of the S₁ and S₁* states and begin by considering the energetics of these states. Electronic structure calculations indicate that in all cases, the optical excitations correspond to a $\pi \rightarrow \pi^*$, HOMO-to-LUMO transition. Starting with the optimized ground-state geometries (Table S4), the computed vertical transition energies of **T3** and **T3SOₙT3** are in reasonable agreement with the experimental absorption maxima in dichloromethane and properly reflect the relative shift observed when increasing the oxidation state of the linker (Table 3). The absorption redshift of **T3SOₙMe** with

Table 3. Experimental Absorption Maxima and Computed Vertical Excitation Energies to the Lowest Excited Singlet State of T3, T3SOₙMe, and T3SOₙT3 Molecules in Dichloromethane Solution[a]

	molecule				
λ_{max} (nm)	T3	T3SO₂Me	T3ST3	T3SOT3	T3SO₂T3
experimental	350	370	374	371	410
calculated	348	362	366	371	380

[a]All values are in nm.

respect to **T3** can be rationalized, to a first approximation, as a result of LUMO stabilization due to the bonding interaction of the **T3** fragment with the SOₙ bridge. This effect increases with the oxidation state of the sulfur atom in the linker group. Oxidation of the sulfur atom also results in stabilization of the HOMO, but this effect is smaller than the energy lowering of the LUMO (Figures S21 and S22). The excited states for all monomer molecules are qualitatively the same, involving a neutral state similar to that of **T3**.
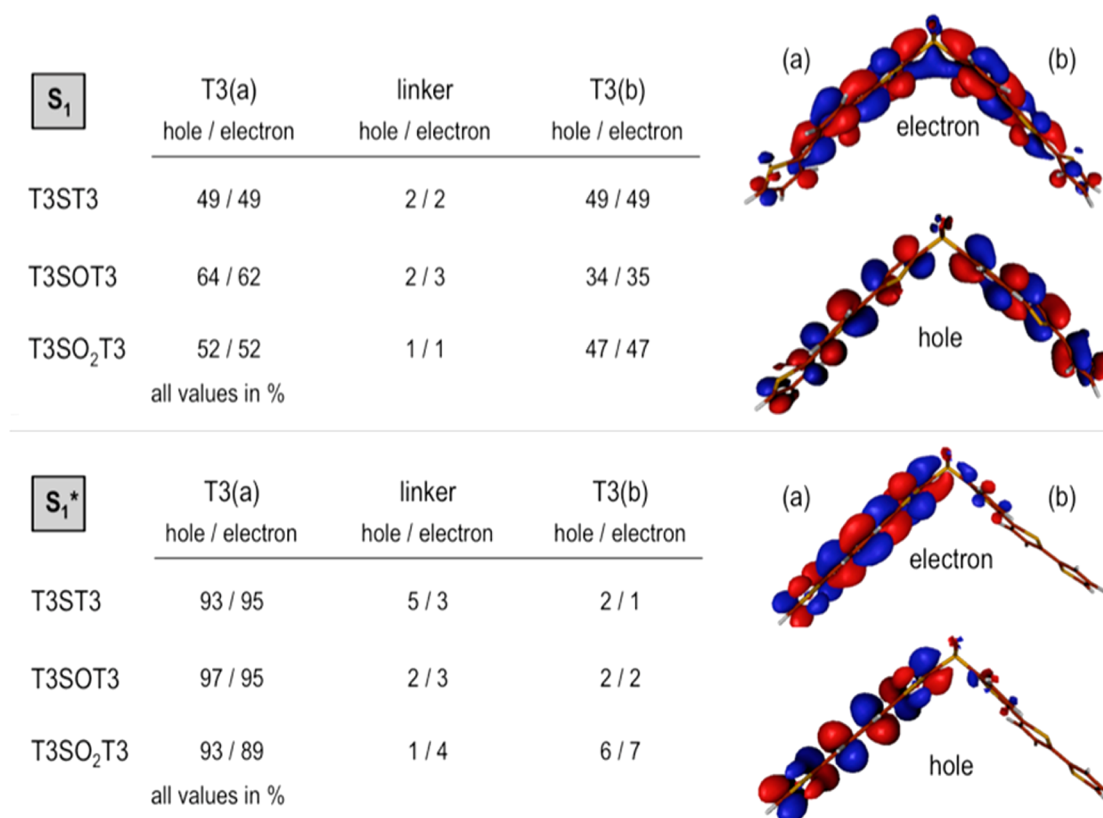
When the excited states are calculated for the optimized ground-state geometries of the **T3SOₙT3** series, we find that the lowest excited singlet state (S₁) can be described, to a first approximation, as the coupling of local excitons on each of the **T3** fragments. In symmetric dimers, the strength of this electronic interaction can be quantified by the orbital energy gap between the HOMO and HOMO−1 (ΔHOMO), the LUMO and LUMO+1 (ΔLUMO) and the exciton splitting energy $\Delta\varepsilon$ (Figure S23). Table 4 reports orbital energy differences and computed exciton splitting energies for the *cis* and *trans* conformers of the **T3SOₙT3** dimers (Figure S24).

For the *cis* conformers, the calculated values follow similar trends as the measured $\Delta\varepsilon$ values with respect to sulfur

Table 4. Computed Orbital Energy Gaps ΔHOMO and ΔLUMO and Exciton Splitting Δε (in cm⁻¹) for the T3SOₙT3 Series in Dichloromethane[a]

		molecule		
	parameter	T3ST3	T3SOT3	T3SO₂T3
trans	ΔHOMO (cm⁻¹)	1114	929	1400
	ΔLUMO (cm⁻¹)	909	1374	3053
	$\Delta\varepsilon$ (cm⁻¹)	1057	951	1430
cis	ΔHOMO (cm⁻¹)	615	835	1784
	ΔLUMO (cm⁻¹)	1148	1722	3518
	$\Delta\varepsilon$ (cm⁻¹)	238	1098	1731

[a]Ground-state energy differences between *cis* and *trans* conformers of **T3SOₙT3** are in the order of 1 kcal/mol, with the *trans* form being the most stable structure in the three dimers.

S_1	T3(a) hole / electron	linker hole / electron	T3(b) hole / electron
T3ST3	49 / 49	2 / 2	49 / 49
T3SOT3	64 / 62	2 / 3	34 / 35
T3SO$_2$T3	52 / 52	1 / 1	47 / 47

all values in %

S_1*	T3(a) hole / electron	linker hole / electron	T3(b) hole / electron
T3ST3	93 / 95	5 / 3	2 / 1
T3SOT3	97 / 95	2 / 3	2 / 2
T3SO$_2$T3	93 / 89	1 / 4	6 / 7

all values in %

Figure 8. Fragment localization of the lowest singlet exciton of the **T3SO$_n$T3** dimers in dichloromethane and electron and hole NTOs accounting for 70% of the electronic transition in **T3SO$_2$T3** (top). Fragment localization of the lowest singlet exciton of the **T3SO$_n$T3** dimers for the S_1* optimized geometries in dichloromethane and electron and hole NTOs (bottom). The percentage of hole and electron exciton on each fragment (exciton localization) is obtained through NTO analysis.[60]

oxidation state, with the strongest exciton coupling obtained for the SO$_2$ linker. For the *trans* conformers, the **T3SOT3** dimer is the only case where the two **T3** moieties are not equivalent due to the absence of a C_2 axis and there is a deviation from the trend of symmetric dimers. The computed differences in energy for the ground-state *cis* and *trans* conformers are small (less than kT), and it is likely that there is a statistical mixture of these conformers in solution.

When the S_1 excited states of the dimers are examined in detail, several noteworthy features emerge. In all three **T3SO$_n$T3** dimers, the electron–hole pair of the S_1 state fully delocalizes over the two **T3** fragments with minor contributions from the SO$_n$ bridge, as characterized by means of a natural transition orbital (NTO) analysis (Figure 8, top).[60] Although the S_1 state is delocalized in all three dimers, exciton decomposition in terms of two LE and two CT diabatic states highlights the distinctive nature of the S_1 state in **T3SO$_2$T3** with respect to **T3ST3** and **T3SOT3**. The lowest exciton for the S and SO bridged dimers exhibits strong neutral character with ≤5% of CT participation, but in **T3SO$_2$T3** CT contributions account for 35% of the wave function (Table 5). The energy gap between the lowest neutral and CT states in **T3ST3** and **T3SOT3** is ~1.0 eV, while it reduces to ~0.5 eV for **T3SO$_2$T3**. This leads to neutral-CT couplings that are much larger for **T3SO$_2$T3**. It is important that due to the symmetry of the dimers, opposite CT contributions in these species are degenerate (charge resonance, CR), resulting in no net electron transfer between **T3** moieties (Figure S25). This could explain the weak dependence of the absorbance peak with solvent polarity.

Table 5. Computed CT Contributions, Energy Gap between the Lowest Neutral and CT Diabatic States and Their Absolute Electronic Coupling for the S_1 State in the T3SO$_n$T3 Series at Their Optimized and T3SO$_2$T3-Like Geometries

		molecule		
	parameter	T3ST3	T3SOT3	T3SO$_2$T3
optimized geometry	% CT	5	1	35
	ΔE (eV)	1.00	0.95	0.53
	neutral-CT coupling (meV)	149	41	429
T3SO$_2$T3 geometry	% CT	7	8	35
	ΔE (eV)	0.98	0.79	0.53
	neutral-CT coupling (meV)	238	269	429

Experimentally, absorption to S_1 does not involve a large change in the net dipole moment, but geometrical relaxation to S_1* clearly does, as evidenced by the strong solvatochromism of this state. In order to gain insight into the formation of the S_1* state, the electronic structure of each dimer was calculated after allowing them to fully relax in their first excited state (Table 6). We find that molecular relaxation on the S_1 potential energy surface localizes the exciton onto one of the **T3** fragments for all **T3SO$_n$T3** molecules. Comparing the S_1 state (Figure 8, top) to the S_1* state (Figure 8, bottom) shows that relaxation induces a symmetry breaking where one of the **T3** planarizes, localizing the charge and collapsing the CR state.[11,61,62] The bottom panel of Figure 8 shows that there is now a net partial

Table 6. Atomic Charges and Electron Occupancies of $3p_x$, $3p_y$, and $3p_z$ Bridging Sulfur Atom (S) Orbitals at the SO_n, SH_4, and SF_4 Bridges Obtained from NBO Analysis at the CAM-B3LYP/6-31+G(d) Level in Dichloromethane

		molecule				
		T3ST3	T3SOT3	T3SO$_2$T3	T3SH$_4$T3	T3SF$_4$T3
charge	bridging S	0.351	1.383	2.269	0.655	2.322
	X[a]	–	−1.023	−0.985	−0.003/0.021	−0.518/-0.510
electron occupancy	3p	3.99	3.06	2.50	3.85	2.37
	3p$_x$/3p$_z$	1.82/1.27	1.14/1.03	0.72/0.85	1.37/1.23	0.66/0.82
	3p$_y$	0.89	0.89	0.93	1.25	0.90

[a]X = O, H, F.

electron transfer to the other **T3**. The S_1^* state thus has a net dipole and can be thought of as a true CT state. Surprisingly, the overall CT contribution at the S_1^* optimized geometry of **T3SO$_2$T3** in dichloromethane is on the order of 25%, slightly lower in comparison to the 35% computed at the ground-state geometry (Table S6). However, the most important difference is that in the ground-state geometry, the CT character is symmetrically shared between the two **T3** fragments, while in the S_1^* structure 22% is localized on one **T3** fragment and 3% on the other.

The CR/CT character of the S_1^* state provides a qualitative explanation for the longer fluorescence lifetimes of the dimers. In **T3**, the lowest excited singlet decays rapidly to a high-lying triplet state which has been variously assigned as T_2 or T_4.[59,63,64] This state then internally converts to the lowest triplet state T_1 on a subpicosecond time scale. This ISC process limits the fluorescence quantum yield of **T3** to 5% or less in solution. In the dimers, our calculations indicate that the triplet levels on separate **T3** chromophores combine to form new excitonic states. These new excitonic states are denoted T_1 and T_1' (from mixing the original T_1 states on different **T3**'s), while T_2 and T_2' arise from mixing the original T_2 states on different **T3**'s (Figure S26). The excitonic T_1, T_1', T_2, and T_2' triplet states are all close in energy to the S_1/S_1^* states, and calculations indicate that all these states have predominantly neutral character. Due to the one electron nature of the spin−orbit operator, CT contributions to S_1/S_1^* cannot couple to the neutral terms in the triplet-state wave functions. If the S_1 state in the dimer has a pure neutral character, the ISC rate should be similar to that of **T3**. Increasing the CR/CT character of S_1/S_1^* should lead to less effective singlet−triplet coupling and less efficient ISC. This reasoning has also been used to rationalize the decreased ISC rates in oligothiophenes[54,59] and helps explain the increased fluorescence as the sulfur linker is oxidized from S to SO to SO_2. The ISC rate in the dimeric species also decreases with increasing solvent polarity from cyclohexane to dichloromethane. This behavior can again be rationalized in terms of increased CT mixing in the lowest exciton. This trend of increasing CT state mixing does not explain the shorter fluorescence lifetime in acetonitrile, however. It is likely that other factors affect the lifetime of the S_1^* state in highly polar solvents, for example, the smaller S_0–S_1^* and S_1^*−T_1 energy gaps that could facilitate more rapid internal conversion or ISC.

The overall picture of the excited-state dynamics that emerges is summarized schematically in Figure 9. Photoexcitation leads to an excitonic S_1 state with symmetric CR character that relaxes rapidly (<10 ps) to an asymmetric S_1^* state with strong CT character. Although we have mapped out the excited-state structure of the dimers, the question remains
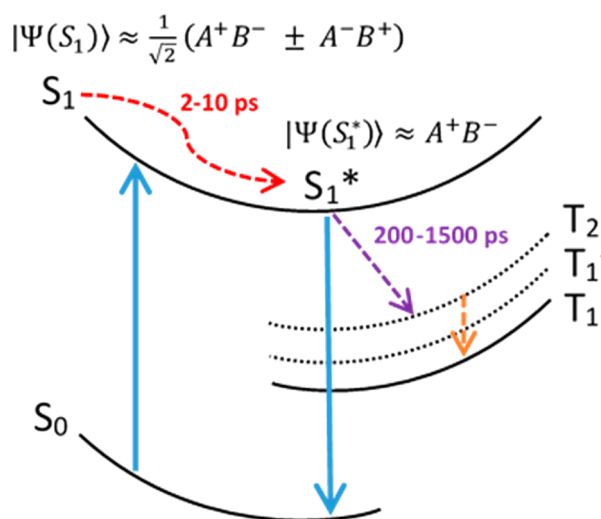
Figure 9. Schematic illustration of excited-state relaxation in the dimers. Note that the S_1 and S_1^* states are in general superposition states with contributions from both CT and neutral states. We show the dominant CT terms to emphasize the symmetry breaking between the two states.

as to how the oxidation state of sulfur controls the amount of CT character. Below, we consider two possible mechanisms.

One mechanism by which the sulfur oxidation state could affect the electronic coupling is through inducing changes in the dimer geometry. To investigate the impact of the molecular geometry on the S_1 state, the **T3ST3** and **T3SOT3** dimers were constrained to adopt the **T3SO$_2$T3** optimized geometry (Table 5), and their lowest electronic transitions were analyzed. The results obtained for these models, both regarding the CT character of the electronic transition and the neutral-CT energy difference, are similar to the values obtained for **T3ST3** and **T3SOT3** with their own optimized geometries. That is to say, changes in the **T3SO$_2$T3** geometry cannot explain the enhanced CT character of the S_1 state. Moreover, the data in Table 5 show that when the relative arrangement of the two **T3** units is fixed, a clear correlation between the exciton splitting $\Delta\varepsilon$ and the oxidation state of the sulfur atom in the linker emerges (one that follows the experimental data closely).

A second possible mechanism for the changes in electronic coupling involves different Coulombic interactions. A major electronic structure difference between the SO_2 bridge and the S and SO linkers is the absence of sulfur lone pairs in the former. To investigate this difference in more detail, we evaluate the electronic structure at the SO_n linkers in the **T3SO$_n$T3** dimers by means of a NBO analysis.[65] Table 6 summarizes the most relevant results obtained. The charge of the bridging sulfur atom increases with oxidation state, while

the oxygen charge remains almost constant. This behavior is a consequence of the strong polarity of the SO bonds toward the oxygen atom, as indicated by the decrease in the electronic occupation of p orbitals involved in the SO bonds ($3p_x$ and $3p_z$) and constant occupation of the p orbital oriented in the perpendicular direction ($3p_y$). In other words, the oxygen atoms pull electron density away from the sulfur atom in the bridge. These results are in line with a study of the nature of bonding in sulfoxide and sulfone systems by Chesnut and Quin.[66]

To further explore the impact of the electronic configuration of the sulfur atom in the bridge, we computed the neutral-CT mixing and electronic couplings for two additional **T3** dimers, **T3SH$_4$T3** and **T3SF$_4$T3**. As in the SO$_2$ case, the SH$_4$ and SF$_4$ linkers lack electron lone pairs on the sulfur atom, but represent very different situations with respect to the polarization of the SX bonds. NBO analysis shows that the electron occupation of the 3p level of the sulfur atom in SH$_4$ (3.85 electrons) is of the same magnitude as that in **T3ST3**, while in **T3SF$_4$T3** the electron density is polarized toward the fluorine atoms (2.37 electrons in the 3p level). As a result, **T3SH$_4$T3** exhibits strong electronic screening, similar to that in the **T3ST3** dimer, while the neutral-CT mixing and coupling obtained for the SF$_4$ linker is similar to that of the SO$_2$ bridge (Figure 10). Decreased CT
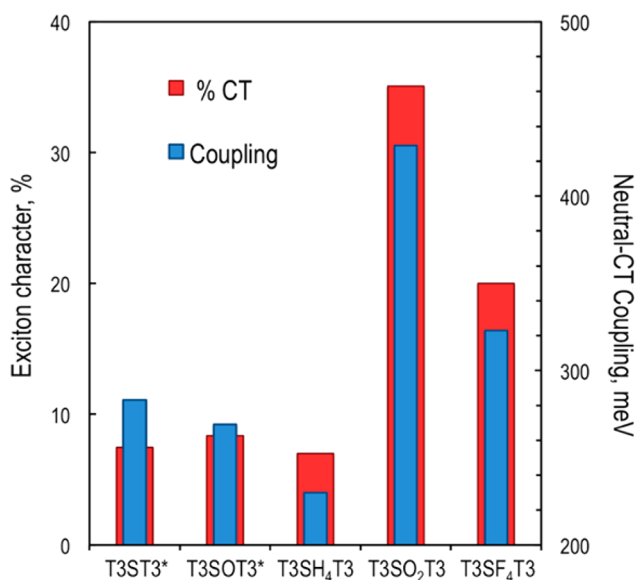
Figure 10. Exciton character as contributions (in %) of CT diabatic states to S$_1$ transition (red wide bars) and neutral-CT couplings (blue thin bars) for the **T3SO$_2$T3**, **T3SH$_4$T3**, and **T3SF$_4$T3** dimers and the **T3ST3*** and **T3SOT3*** molecular models obtained at the CAM-B3LYP/6-31+G(d) computational level in dichloromethane.

coupling was also observed when the linker was changed to an O atom, which has lone pairs, while a CH$_2$ linker (with no lone pairs) resulted in a CT coupling comparable to the SO$_2$ linker (Figure S27).These results suggest that the electronic configuration of the sulfur atom in the SO$_n$ bridge is the key factor that can suppress or enhance the neutral-CT mixing. In particular, we conclude that the presence of electron lone pairs in the bridge can screen Coulombic interactions between **T3** moieties and suppress intradimer electronic coupling that stabilizes delocalized CR states. We also suggest that the polarization of the SO bonds has a major role in this mechanism and that in SX$_4$ linkers, with formally no available

electron lone pairs on the sulfur atom, polarization of the SX bonds dictates the screening strength of the electronic interactions between the **T3** moieties.

4. DISCUSSION

The first important point of this paper is that the sulfur bridge itself has only a minor effect on the behavior of the molecule. For example, in the **T3SO$_n$Me** monomers, the presence of the additional sulfur functionality leads to a slight (~20 nm) red-shift of the absorption spectrum in the monomer series (**T3SO$_n$Me**) relative to unsubstituted **T3**, while the overall shape of the spectrum remains largely unchanged. The PL lifetime (τ_{PL}) of the **T3SO$_2$Me** monomer is nearly identical to that of unsubstituted **T3** (~200 ps). The **T3SO$_n$Me** monomer series exhibits very similar features in the TA data to that of **T3**. As in **T3**, the excited state of the monomers evolves from an S$_1$ state with predominantly neutral character to T$_1$ through ISC. The addition of a second **T3** chromophore generates qualitative changes in the electronic structure and photophysics of the dimers. The appearance of a splitting in the dimer absorption is a clear indication that interaction between the two absorbing units has an important role in the excited-state dynamics. The solvatochromism in the steady-state fluorescence behavior of the dimers, which is absent in the monomers, indicates stabilization of a polarized CT excited-state, denoted S$_1$*, that is present only in the S-bridged dimers. This CT state leads to a fluorescence lifetime and quantum yield for the dimer (**T3SO$_2$T3**) that are significantly greater than those of **T3SO$_2$Me** or unsubstituted **T3**.

The second major finding is the dynamic nature of the S$_1$* state, which is formed within 10 ps, consistent with relaxation via symmetry breaking. The ability of an initially delocalized system to relax into an asymmetric charge distribution is an interesting fundamental process[67] and has been characterized in several types of multichromophoric systems,[10−12,62,68,69] including bianthryl.[61] Common features in the photophysics of this class of molecules include the shift of the CT emission with solvent polarity, with no shift in absorption, and the rapid relaxation from the neutral absorption state to the CT emitting state. However, there are also some notable differences between our sulfur-bridged dimers and the prototypical bichromophore, bianthryl. In bianthryl, the absorption spectrum closely resembles that of monomeric anthracene. The initial excited state of bianthryl is assumed to be localized on one of the anthracenes and is referred to as the "locally excited" (LE) state. In the **T3** dimers, the two chromophores have significant interactions even in the ground-state configuration, as evaluated from the changes in the absorption spectra. This is likely the result of the following: the larger transition dipole moment of the **T3** chromophore, the sulfur bridge orienting the transition dipole moments of the chromophores at an oblique angle, and more facile electron-transfer interactions through the bridge. Strong interchromophore interactions are in a sense built into our sulfur-bridged dimers. A second major difference is that **T3**, unlike anthracene, has a very low fluorescence quantum yield to begin with due to rapid ISC. Typically, the quantum yield of dimeric anthracenes decreases relative to the monomer due to the lower radiative rate of the dimer CT state.[70,71] In the **T3** dimers, the lower ISC rate in the CT state more than compensates for the decrease in radiative rate, and the fluorescence quantum yield increases by an order of magnitude for **T3SO$_2$T3** in dichloromethane.

The most obvious difference between the sulfur-bridged dimers and bianthryl is the ability to tune the amount of electronic coupling by changing the oxidation state of the bridging sulfur. The computational results indicate that the electron lone pairs present in the S and SO bridges screen the interaction between the π electrons from the two **T3** chromophores. Oxidation of the sulfur atom to form the sulfone (SO_2) linker leads to polarized bonds that decrease this screening, stabilizing the CT contributions that mix with the neutral states. It might naively be expected that greater electron density on the sulfur would facilitate electronic communication between the **T3** chromophores, but our results show that the opposite occurs. The role of solvent in screening electrostatic interactions between different regions of molecules that undergo electron transfer has been the subject of theoretical attention,[72,73] but the possibility that the polarization of the bridge valence electrons can modulate interchromophore electronic interactions has not been a significant focus.[74] Both our experimental and computational results provide evidence that the electron distribution on the bridge atom can suppress the electrostatic interactions that stabilize a luminescent CT state, suggesting that this may be an effective strategy to explore in molecular design.

The ability of the SO_2 linker to facilitate the formation of CT states may explain its utility in chromophores that exhibit TADF, where CT interactions lead to small exchange energies and near degeneracy of the singlet and triplet states.[15,16] Oxidizing the sulfur in polythiophenes has also been shown to be an effective way to modulate the polymer bandgap,[75] most likely due to the creation of extended CT states. Our results provide an explanation for these results and, furthermore, show that formation of CT states can suppress ISC and lead to higher fluorescence quantum yields. The SO_2 linker has the added advantage of being stable against further oxidation.

While enhancement of CT interactions led to a high PL yield in our **T3** dimers, it is possible that this approach can be used in other systems to suppress CT formation. For example, if the chromophore neutral states are highly emissive (i.e., not subject to rapid ISC), then one would want to avoid CT mixing that lowers the radiative rate. To make a superradiant assembly of such chromophores,[76] one would want to use the unoxidized S linker in order to prevent CT state formation. Another application for tuning the amount of CT interaction would be to optimize singlet fission. There is general agreement that efficient singlet fission requires some CT interaction,[77−80] but too much CT character can lead to excimer formation that competes with the fission channel. Although the examples given above are somewhat speculative, they serve to illustrate how controlling interchromophore interactions in covalent assemblies could be useful for the design of functional supermolecules.

5. CONCLUSION

In this paper, we have combined spectroscopy and computation to obtain a comprehensive picture of the photodynamics of sulfur-bridged terthiophene dimers. Their novel excited-state behaviors (high fluorescence quantum yields, solvatochromism, two-step excited-state relaxation) stem from the formation of a delocalized CR state (S_1) that relaxes quickly (<10 ps) to a CT state (S_1*). The amount of CT in S_1 and S_1* can be modified by changing the oxidation state of the bridging sulfur group. Computational work indicates that electrostatic screening by the sulfur valence electrons is the key parameter that controls

the amount of CT participation. The results presented in this paper provide a new strategy for tuning interchromophore interactions in covalent dimers.

■ ASSOCIATED CONTENT

ⓢ Supporting Information

The Supporting Information is available free of charge on the ACS Publications website at DOI: 10.1021/jacs.5b05457.

Experimental details, characterization, supplementary figures, tables, and discussion (PDF)

■ AUTHOR INFORMATION

Corresponding Authors
*david.casanova@ehu.es
*mwolf@chem.ubc.ca
*christopher.bardeen@ucr.edu

Author Contributions
∥These authors contributed equally.

Notes
The authors declare no competing financial interest.

■ REFERENCES

(1) Ricks, A. B.; Brown, K. E.; Wenninger, M.; Karlen, S. D.; Berlin, Y. A.; Co, D. T.; Wasielewski, M. R. *J. Am. Chem. Soc.* **2012**, *134*, 4581.

(2) Mathew, S.; Yella, A.; Gao, P.; Humphry-Baker, R.; CurchodBasile, F. E.; Ashari-Astani, N.; Tavernelli, I.; Rothlisberger, U.; NazeeruddinMd, K.; Grätzel, M. *Nat. Chem.* **2014**, *6*, 242.

(3) Cheng, Y.-C.; Fleming, G. R. *Annu. Rev. Phys. Chem.* **2009**, *60*, 241.

(4) Collini, E.; Wong, C. Y.; Wilk, K. E.; Curmi, P. M. G.; Brumer, P.; Scholes, G. D. *Nature* **2010**, *463*, 644.

(5) Clayton, A. H. A.; Scholes, G. D.; Ghiggino, K. P.; Paddon-Row, M. N. *J. Phys. Chem.* **1996**, *100*, 10912.

(6) Curutchet, C.; Mennucci, B. *J. Am. Chem. Soc.* **2005**, *127*, 16733.

(7) Zhong, Y.; Trinh, M. T.; Chen, R.; Wang, W.; Khlyabich, P. P.; Kumar, B.; Xu, Q.; Nam, C.-Y.; Sfeir, M. Y.; Black, C.; Steigerwald, M. L.; Loo, Y.-L.; Xiao, S.; Ng, F.; Zhu, X. Y.; Nuckolls, C. *J. Am. Chem. Soc.* **2014**, *136*, 15215.

(8) Zhang, X.; Lu, Z.; Ye, L.; Zhan, C.; Hou, J.; Zhang, S.; Jiang, B.; Zhao, Y.; Huang, J.; Zhang, S.; Liu, Y.; Shi, Q.; Liu, Y.; Yao, J. *Adv. Mater.* **2013**, *25*, 5791.

(9) Kang, T. J.; Kahlow, M. A.; Giser, D.; Swallen, S.; Nagarajan, V.; Jarzeba, W.; Barbara, P. F. *J. Phys. Chem.* **1988**, *92*, 6800.

(10) Whited, M. T.; Patel, N. M.; Roberts, S. T.; Allen, K.; Djurovich, P. I.; Bradforth, S. E.; Thompson, M. E. *Chem. Commun.* **2012**, *48*, 284.

(11) Trinh, C.; Kirlikovali, K.; Das, S.; Ener, M. E.; Gray, H. B.; Djurovich, P.; Bradforth, S. E.; Thompson, M. E. *J. Phys. Chem. C* **2014**, *118*, 21834.

(12) Bartynski, A. N.; Gruber, M.; Das, S.; Rangan, S.; Mollinger, S.; Trinh, C.; Bradforth, S. E.; Vandewal, K.; Salleo, A.; Bartynski, R. A.; Bruetting, W.; Thompson, M. E. *J. Am. Chem. Soc.* **2015**, *137*, 5397.

(13) Wohlgenannt, M.; Tandon, K.; Mazumdar, S.; Ramasesha, S.; Vardeny, Z. V. *Nature* **2001**, *409*, 494.

(14) Segal, M.; Singh, M.; Rivoire, K.; Difley, S.; Van Voorhis, T.; Baldo, M. A. *Nat. Mater.* **2007**, *6*, 374.

(15) Endo, A.; Sato, K.; Yoshimura, K.; Kai, T.; Kawada, A.; Miyazaki, H.; Adachi, C. *Appl. Phys. Lett.* **2011**, *98*, 083302.

(16) Uoyama, H.; Goushi, K.; Shizu, K.; Nomura, H.; Adachi, C. *Nature* **2012**, *492*, 234.

(17) Sato, K.; Shizu, K.; Yoshimura, K.; Kawada, A.; Miyazaki, H.; Adachi, C. *Phys. Rev. Lett.* **2013**, *110*, 247401.

(18) Zhang, Q.; Li, J.; Shizu, K.; Huang, S.; Hirata, S.; Miyazaki, H.; Adachi, C. *J. Am. Chem. Soc.* **2012**, *134*, 14706.

(19) Zhang, Q.; Li, B.; Huang, S.; Nomura, H.; Tanaka, H.; Adachi, C. *Nat. Photonics* **2014**, *8*, 326.

(20) Xu, B.; Holdcroft, S. *Macromolecules* **1993**, *26*, 4457.

(21) Christensen, P. R.; Nagle, J. K.; Bhatti, A.; Wolf, M. O. *J. Am. Chem. Soc.* **2013**, *135*, 8109.

(22) *Surface Xplorer*; Ultrafast Systems LLC: Sarasota, FL, 2010.

(23) Parr, R. G.; Yang, W. *Density Functional Theory of Atoms and Molecules*; Oxford University Press, New York, 1994.

(24) Ziegler, T. *Chem. Rev.* **1991**, *91*, 651.

(25) Yanai, T.; Tew, D. P.; Handy, N. C. *Chem. Phys. Lett.* **2004**, *393*, 51.

(26) Mark, E. C. In *Recent Advances in Density Functional Methods*; World Scientific: Singapore, 1995; Vol. 1, p 155.

(27) Runge, E.; Gross, E. K. U. *Phys. Rev. Lett.* **1984**, *52*, 997.

(28) Fetter, A. L.; Walecka, J. D. *Quantum Theory of Many Particle Systems*; Dover Publications: Mineola, NY, 2003.

(29) Hirata, S.; Head-Gordon, M. *Chem. Phys. Lett.* **1999**, *314*, 291.

(30) Fabian, J. *Theor. Chem. Acc.* **2001**, *106*, 199.

(31) Preat, J. *J. Phys. Chem. C* **2010**, *114*, 16716.

(32) Camino, B.; De La Pierre, M.; Ferrari, A. M. *J. Mol. Struct.* **2013**, *1046*, 116.

(33) Jungsuttiwong, S.; Tarsang, R.; Sudyoadsuk, T.; Promarak, V.; Khongpracha, P.; Namuangruk, S. *Org. Electron.* **2013**, *14*, 711.

(34) Truong, T. N.; Stefanovich, E. V. *Chem. Phys. Lett.* **1995**, *240*, 253.

(35) Subotnik, J. E.; Cave, R. J.; Steele, R. P.; Shenvi, N. *J. Chem. Phys.* **2009**, *130*, 234102.

(36) Shao, Y.; Gan, Z.; Epifanovsky, E.; Gilbert, A. T. B.; Wormit, M.; Kussmann, J.; Lange, A. W.; Behn, A.; Deng, J.; Feng, X.; Ghosh, D.; Goldey, M.; Horn, P. R.; Jacobson, L. D.; Kaliman, I.; Khaliullin, R. Z.; Kuś, T.; Landau, A.; Liu, J.; Proynov, E. I.; Rhee, Y. M.; Richard, R. M.; Rohrdanz, M. A.; Steele, R. P.; Sundstrom, E. J.; Woodcock, H. L.; Zimmerman, P. M.; Zuev, D.; Albrecht, B.; Alguire, E.; Austin, B.; Beran, G. J. O.; Bernard, Y. A.; Berquist, E.; Brandhorst, K.; Bravaya, K. B.; Brown, S. T.; Casanova, D.; Chang, C.-M.; Chen, Y.; Chien, S. H.; Closser, K. D.; Crittenden, D. L.; Diedenhofen, M.; DiStasio, R. A.; Do, H.; Dutoi, A. D.; Edgar, R. G.; Fatehi, S.; Fusti-Molnar, L.; Ghysels, A.; Golubeva-Zadorozhnaya, A.; Gomes, J.; Hanson-Heine, M. W. D.; Harbach, P. H. P.; Hauser, A. W.; Hohenstein, E. G.; Holden, Z. C.; Jagau, T.-C.; Ji, H.; Kaduk, B.; Khistyaev, K.; Kim, J.; Kim, J.; King, R. A.; Klunzinger, P.; Kosenkov, D.; Kowalczyk, T.; Krauter, C. M.; Lao, K. U.; Laurent, A. D.; Lawler, K. V.; Levchenko, S. V.; Lin, C. Y.; Liu, F.; Livshits, E.; Lochan, R. C.; Luenser, A.; Manohar, P.; Manzer, S. F.; Mao, S.-P.; Mardirossian, N.; Marenich, A. V.; Maurer, S. A.; Mayhall, N. J.; Neuscamman, E.; Oana, C. M.; Olivares-Amaya, R.; O'Neill, D. P.; Parkhill, J. A.; Perrine, T. M.; Peverati, R.; Prociuk, A.; Rehn, D. R.; Rosta, E.; Russ, N. J.; Sharada, S. M.; Sharma, S.; Small, D. W.; Sodt, A.; Stein, T.; Stück, D.; Su, Y.-C.; Thom, A. J. W.; Tsuchimochi, T.; Vanovschi, V.; Vogt, L.; Vydrov, O.; Wang, T.; Watson, M. A.; Wenzel, J.; White, A.; Williams, C. F.; Yang, J.; Yeganeh, S.; Yost, S. R.; You, Z.-Q.; Zhang, I. Y.; Zhang, X.; Zhao, Y.; Brooks, B. R.; Chan, G. K. L.; Chipman, D. M.; Cramer, C. J.; Goddard, W. A.; Gordon, M. S.; Hehre, W. J.; Klamt, A.; Schaefer, H. F.; Schmidt, M. W.; Sherrill, C. D.; Truhlar, D. G.; Warshel, A.; Xu, X.; Aspuru-Guzik, A.; Baer, R.; Bell, A. T.; Besley, N. A.; Chai, J.-D.; Dreuw, A.; Dunietz, B. D.; Furlani, T. R.; Gwaltney, S. R.; Hsu, C.-P.; Jung, Y.; Kong, J.; Lambrecht, D. S.; Liang, W.; Ochsenfeld, C.;

Rassolov, V. A.; Slipchenko, L. V.; Subotnik, J. E.; Van Voorhis, T.; Herbert, J. M.; Krylov, A. I.; Gill, P. M. W.; Head-Gordon, M. *Mol. Phys.* **2015**, *113*, 184.

(37) Glendening, E. D. B, J. K.; Reed, A. E.; Carpenter, J. E.;Bohmann, J. A.;Morales, C. M.;Weinhold, F. *NBO 5.0 package*; Theoretical Chemistry Institute, University of Wisconsin: Madison, WI, 2001.

(38) Grebner, D.; Helbig, M.; Rentsch, S. *J. Phys. Chem.* **1995**, *99*, 16991.

(39) Yassar, A.; Horowitz, G.; Valat, P.; Wintgens, V.; Hmyene, M.; Deloffre, F.; Srivastava, P.; Lang, P.; Garnier, F. *J. Phys. Chem.* **1995**, *99*, 9155.

(40) Kasha, M. *Radiat. Res.* **1963**, *20*, 55.

(41) Kasha, M.; Rawls, H. R.; Ashraf El-Bayoumi, M. *Pure Appl. Chem.* **1965**, *11*, 371.

(42) Spano, F. C. *Acc. Chem. Res.* **2010**, *43*, 429.

(43) Van Bolhuis, F.; Wynberg, H.; Havinga, E. E.; Meijer, E. W.; Staring, E. G. J. *Synth. Met.* **1989**, *30*, 381.

(44) Kouki, F.; Spearman, P.; Valat, P.; Horowitz, G.; Garnier, F. *J. Chem. Phys.* **2000**, *113*, 385.

(45) Beenken, W. J. D.; Pullerits, T. *J. Chem. Phys.* **2004**, *120*, 2490.

(46) Krueger, B. P.; Scholes, G. D.; Fleming, G. R. *J. Phys. Chem. B* **1998**, *102*, 5378.

(47) Scholes, G. D. *Annu. Rev. Phys. Chem.* **2003**, *54*, 57.

(48) Wong, K. F.; Bagchi, B.; Rossky, P. J. *J. Phys. Chem. A* **2004**, *108*, 5752.

(49) Harcourt, R. D.; Ghiggino, K. P.; Scholes, G. D.; Speiser, S. *J. Chem. Phys.* **1996**, *105*, 1897.

(50) Harcourt, R. D.; Scholes, G. D.; Ghiggino, K. P. *J. Chem. Phys.* **1994**, *101*, 10521.

(51) Scholes, G. D.; Harcourt, R. D.; Ghiggino, K. P. *J. Chem. Phys.* **1995**, *102*, 9574.

(52) Thompson, A. L.; Gaab, K. M.; Xu, J.; Bardeen, C. J.; Martinez, T. J. *J. Phys. Chem. A* **2004**, *108*, 671.

(53) Rossi, R.; Ciofalo, M.; Carpita, A.; Ponterini, G. *J. Photochem. Photobiol., A* **1993**, *70*, 59.

(54) Becker, R. S.; Seixas de Melo, J.; Maçanita, A. L.; Elisei, F. *J. Phys. Chem.* **1996**, *100*, 18683.

(55) Bixon, M.; Jortner, J.; Verhoeven, J. W. *J. Am. Chem. Soc.* **1994**, *116*, 7349.

(56) Gould, I. R.; Young, R. H.; Mueller, L. J.; Albrecht, A. C.; Farid, S. *J. Am. Chem. Soc.* **1994**, *116*, 8188.

(57) Paa, W.; Yang, J. P.; Rentsch, S. *Appl. Phys. B: Lasers Opt.* **2000**, *71*, 443.

(58) Reyftmann, J. P.; Kagan, J.; Santus, R.; Morliere, P. *Photochem. Photobiol.* **1985**, *41*, 1.

(59) Beljonne, D.; Cornil, J.; Friend, R. H.; Janssen, R. A. J.; Brédas, J. L. *J. Am. Chem. Soc.* **1996**, *118*, 6453.

(60) Martin, R. L. *J. Chem. Phys.* **2003**, *118*, 4775.

(61) Piet, J. J.; Schuddeboom, W.; Wegewijs, B. R.; Grozema, F. C.; Warman, J. M. *J. Am. Chem. Soc.* **2001**, *123*, 5337.

(62) Giaimo, J. M.; Gusev, A. V.; Wasielewski, M. R. *J. Am. Chem. Soc.* **2002**, *124*, 8530.

(63) Rentsch, S.; Yang, J. P.; Paa, W.; Birckner, E.; Schiedt, J.; Weinkauf, R. *Phys. Chem. Chem. Phys.* **1999**, *1*, 1707.

(64) Fabiano, E.; Della Sala, F.; Cingolani, R.; Weimer, M.; Goerling, A. *J. Phys. Chem. A* **2005**, *109*, 3078.

(65) Weinhold, F. L., C.R *Valency and Bonding: A Natural Bond Orbital Donor-Acceptor Perspective*; Cambridge University Press: Cambridge, UK, 2005.

(66) Chesnut, D. B.; Quin, L. D. *J. Comput. Chem.* **2004**, *25*, 734.

(67) Zhang, Q.; Silbey, R. *J. Chem. Phys.* **1990**, *92*, 4899.

(68) Terenziani, F.; Painelli, A.; Katan, C.; Charlot, M.; Blanchard-Desce, M. *J. Am. Chem. Soc.* **2006**, *128*, 15742.

(69) Lewis, F. D.; Daublain, P.; Zhang, L.; Cohen, B.; Vura-Weis, J.; Wasielewski, M. R.; Shafirovich, V.; Wang, Q.; Raytchev, M.; Fiebig, T. *J. Phys. Chem. B* **2008**, *112*, 3838.

(70) Schutz, M.; Schmidt, R. *J. Phys. Chem.* **1996**, *100*, 2012.

(71) Grabner, G.; Rechthaler, K.; Kohler, G. *J. Phys. Chem. A* **1998**, *102*, 689.

(72) Aldern, R. G.; Parson, W. W.; Chu, Z. T.; Warshel, A. *J. Am. Chem. Soc.* **1995**, *117*, 12284.

(73) Lunkenheimer, B.; Kohn, A. *J. Chem. Theory Comput.* **2013**, *9*, 977.

(74) Lu, R.; Lin, J. *Comput. Theor. Chem.* **2014**, *1037*, 10.

(75) Wei, S.; Xia, J.; Dell, E. J.; Jiang, Y.; Song, R.; Lee, H.; Rodenbough, P.; Briseno, A. L.; Campos, L. M. *Angew. Chem., Int. Ed.* **2014**, *53*, 1832.

(76) Spano, F. C.; Mukamel, S. *J. Chem. Phys.* **1989**, *91*, 683.

(77) Greyson, E. C.; Vura-Weis, J.; Michl, J.; Ratner, M. A. *J. Phys. Chem. B* **2010**, *114*, 14168.

(78) Smith, M. B.; Michl, J. *Annu. Rev. Phys. Chem.* **2013**, *64*, 361.

(79) Berkelbach, T. C.; Hybertsen, M. S.; Reichman, D. R. *J. Chem. Phys.* **2013**, *138*, 114102.

(80) Vallett, P. J.; Snyder, J. L.; Damrauer, N. H. *J. Phys. Chem. A* **2013**, *117*, 10824.